Research Square

Preprints are preliminary reports that have not undergone peer review.
They should not be considered conclusive, used to inform clinical practice,
or referenced by the media as validated information.

Dosimetric Comparison of RapidArc Dynamic, VMAT, and IMRT in Left-sided Post-Mastectomy Radiotherapy: Cardiac Substructure Sparing and NTCP Analysis

Yutong Zhao
Shandong Cancer Hospital and Institute, Shandong First Medical University, Shandong Academy of Medical Science

Xinqiang Zhang
Shandong Cancer Hospital and Institute, Shandong First Medical University, Shandong Academy of Medical Science

Xiaoshen Wang
Varian Medical System

Zejun Jiang
Shandong Cancer Hospital and Institute, Shandong First Medical University, Shandong Academy of Medical Science

Jinzhi Wang
Shandong Cancer Hospital and Institute, Shandong First Medical University, Shandong Academy of Medical Science

Haonan Xiao
Shandong Cancer Hospital and Institute, Shandong First Medical University, Shandong Academy of Medical Science

Guanzhong Gong
Shandong Cancer Hospital and Institute, Shandong First Medical University, Shandong Academy of Medical Science

Yong Yin
yinyong@sd-cancer.com

Shandong Cancer Hospital and Institute, Shandong First Medical University, Shandong Academy of Medical Science

---

Research Article

Keywords: Breast Cancer, RapidArc Dynamic, Cardiac substructures, NTCP

Posted Date: September 14th, 2026

DOI: https://doi.org/10.21203/rs.3.rs-10633206/v1

License: This work is licensed under a Creative Commons Attribution 4.0 International License.
Read Full License

Additional Declarations: No competing interests reported.

Abstract

Background

Left-sided breast cancer radiotherapy poses a challenge in balancing target coverage with the sparing of critical cardiac substructures. A novel hybrid technique - RapidArc Dynamic (RAD) - integrated continuous arc delivery of volumetric modulated arc therapy (VMAT) with fixed-beam modulation of intensity modulated radiotherapy (IMRT). Simply put, the radiation machine pauses at strategic angles to deliver highly targeted static beams while rotating, enhancing dose modulation capabilities.

Purpose

This study aims to evaluate the dosimetric performance of RAD, benchmarking it against IMRT and VMAT, with a specific focus on cardiac substructure sparing and normal tissue complication probability (NTCP).

Methods

Twenty patients with left-sided breast cancer treated with post-mastectomy adjuvant radiotherapy were retrospectively enrolled. For each patient, three plans (RAD, IMRT, and VMAT) were generated with a prescription of 50 Gy in 25 fractions; however, five IMRT plans were excluded from comparative analysis due to violations of mean heart dose constraints. RAD plans utilized a “balanced” optimization strategy combining static ports and dynamic arcs with strategic gantry pauses to enhance modulation. Dosimetric metrics were analyzed for the planning target volume (PTV) and organs at risk (OARs). NTCP values were calculated using the Lyman-Kutcher-Burman (LKB) model for multiple endpoints.

Results

Within the subset of compliant plans, RAD demonstrated significantly lower dose metrics for the heart (Dmean: 3.11 Gy vs. 5.78 Gy for IMRT and 5.14 Gy for VMAT, $P < 0.05$), left lung (V20: 19.98% vs. 28.16% for IMRT and 25.10% for VMAT, $P < 0.05$), and spinal cord compared to both IMRT and VMAT. Specifically, RAD achieved superior sparing of the left anterior descending coronary artery (LAD) and left ventricle (LV), reducing mean and maximum doses significantly compared to competing modalities. While VMAT provided better conformity than IMRT, it resulted in a higher low-dose bath to the contralateral breast. Radiobiological modelling demonstrated that RAD successfully mitigated this issue, delivering significantly lower contralateral doses than VMAT (Right lung V_5: 6.76% for RAD vs. 16.58% for VMAT, Right breast V_5: 8.07% vs. 19.57%, $P < 0.05$). RAD yielded significantly lower predicted NTCPs for cardiac perfusion defects, LA major adverse cardiac events, and pulmonary pneumonitis compared to IMRT and VMAT.

Conclusion

RAD offers a promising dosimetric alternative for left-sided post-mastectomy radiotherapy. It demonstrates potential as an advantageous dosimetric technique.

Introduction

Mean heart dose (MHD) has generally served as a primary indicator for assessing the risk of radiation-induced heart disease and structural or functional damage following breast cancer radiotherapy [1–4]. However, given the differential characteristics of cardiac substructures and the heterogeneous dose distributions used in modern radiotherapy, the utility of MHD as the sole predictor of radiation-associated cardiac events has been increasingly questioned [5, 6]. Emerging evidence suggests that dose distribution within specific cardiac substructures may exert a more profound impact on treatment outcomes and cardiotoxicity, particularly in patients with left-sided breast cancer [7–9].

Cardiac substructures exhibit heterogeneity regarding radiosensitivity, dose-response thresholds, and mechanisms of damage. For instance, studies have reported that the maximum dose (D_{max}) to the left anterior descending coronary artery (LAD) exhibits a linear positive correlation with the risk of mortality from ischemic heart disease, as myocardial ischemia in the LAD can directly precipitate anterior wall myocardial infarction [5, 10]. Similarly, incidental irradiation of the left ventricle (LV) may induce long-term chronic damage. A study involving 2,158 patients identified a strong correlation between LV radiation dose and the risk of major ischemic events, likely attributable to radiation-induced myocardial micro-fibrosis, which leads to decreased ventricular compliance and diastolic dysfunction [11]. Consequently, optimizing treatment planning strategies to enhance the protection of specific cardiac substructures is critical for mitigating the risks associated with long-term radiation exposure in breast cancer patients.

As a novel modality, RAD integrates the continuous arc delivery of volumetric modulated arc therapy (VMAT) with the modulation principles of fixed-beam intensity modulated radiotherapy (IMRT). It introduces the capability for the gantry to pause at specific positions while incorporating a dynamically rotating collimator throughout treatment [12]. In a representative left-sided breast cancer case, preliminary research demonstrated that simultaneous integrated boost (SIB) RAD planning achieved a lower MHD, improved dose homogeneity, and better sparing of organs at risk (OARs) compared to VMAT [12]. However, the performance of RAD has not yet been investigated in larger breast cancer cohorts, and existing studies lack a comprehensive evaluation of cardiac substructures.

In contrast to right-sided irradiation, and given the anatomical proximity of the heart to the target volume [13], left-sided breast cancer radiotherapy - specifically left-sided chest wall irradiation - is associated with an elevated incidence of radiation-induced heart disease [4] and non-breast-cancer mortality [14].

This study retrospectively analyzed RAD, IMRT, and VMAT plans for twenty patients. Enrolment was strictly limited to post-mastectomy cases to prevent selection bias and ensure a uniform cohort

representing complex target geometries that challenge cardiac sparing. We hypothesized that RAD provides dosimetrically superior cardiac substructure sparing compared to standard modalities. The primary endpoint was the dosimetric reduction in cardiac substructure metrics, while secondary endpoints included NTCP reduction and target conformity.

Methods and Materials

Data preparation

A total of twenty patients with left-sided breast cancer who underwent post-mastectomy adjuvant external beam radiotherapy (EBRT) at Shandong Cancer Hospital and Institute (Shandong First Medical University, Shandong Academy of Medical Sciences, Jinan, Shandong, China) between January 1, 2024, and January 1, 2025, were retrospectively enrolled in this single-center study. All CT simulations and subsequent treatment plans were performed strictly under free-breathing conditions, as deep inspiration breath hold (DIBH) was not utilized in this specific cohort. Due to the retrospective nature of the study and the use of anonymized patient data, the requirement for free and informed consent was formally waived by the Ethics Committee of Shandong Cancer Hospital.

CT images for all eligible patients were anonymized and collected. Critical OARs including the heart (and its substructures: left atrium (LA), LAD, left circumflex artery (LCX), LV, right atrium (RA), right coronary artery (RCA), right ventricle (RV)), lungs (left and right; upper and lower lobes delineated separately), spinal cord, and oesophagus were initially delineated using the deep learning-based software AccuContour (v3.2, Manteia Technologies Co., Ltd.), which has demonstrated high performance in abdominal and pelvic contouring [15]. All auto-generated contours were subsequently reviewed and manually refined by a medical physicist (XQZ) and a radiology specialist (GZG). The delineation of cardiac substructures (LAD, LCX, chambers) strictly adhered to the consensus guidelines established by Feng et al. [16]. To minimize inter-observer variability, a subset of 5 randomly selected cases was double-checked by a senior radiation oncologist (JZW), with contours adjusted until consensus was reached.

Treatment planning

In this research, target volume delineation followed established international standards (eviQ [17] and NCCN [18]). The clinical target volume (CTV), defined on the planning CT, encompassed the chest wall tissue (skin and invasion regions), internal mammary lymph nodes, mid-axilla (L2), upper-axilla (L3), and supraclavicular lymph nodes. A 5 mm isotropic expansion was applied to the CTV to generate the planning target volume (PTV), accounting for potential setup errors and internal anatomical variations. A 5 mm bolus was applied to the surface of the left chest on the planning CT for all patients.

For each patient, three distinct treatment plans were generated using RAD, IMRT, and VMAT techniques. Planning strictly adhered to standardized OAR dose constraints (Table 1) and dose prescriptions specified by eviQ guidelines [17]. The prescribed dose was 50 Gy delivered to the PTV in 25 fractions.

Clinical acceptability required that a minimum of 95% of the PTV and 99% of the CTV received 100% of the prescribed dose.

Table 1
List of OAR dose constraints.

Organ	Planning Aim	Hard Constraint
Left lung	V_{20} < 15%	V_{20} < 20%
	V_5 < 50%	V_5 < 65%
Right lung	V_5 <10%	V_5 <20%
Heart	V_{20} <5%	V_{20} <10%
		V_{40} < 5%
	D_{mean} <4 Gy	D_{mean} < 8 Gy
Right breast	D_{mean} <2 Gy	D_{mean} <4 Gy
	V_5 < 10%	V_5 < 15%
	V_3 < 10%	
Spinal cord		D_{max} < 45 Gy

D_{max}, D_{mean}: The maximum and average dose of the structure.

V_X: The percentage volume that receives at least x Gy of radiation dose.

All treatment plans were optimized using the Varian Eclipse treatment planning system (Version 18.1, Varian Medical Systems, Palo Alto, CA) for delivery on a Varian TrueBeam linear accelerator. Optimization was performed by a single senior medical physicist (XQZ). To prevent systematic bias, an institutional protocol dictated that equal optimization effort was applied across all modalities until target coverage and OAR sparing were pushed as low as reasonably achievable. A beam energy of 6 MV was utilized for all plans, with dose rates set to 1400 MU/min for RAD and 600 MU/min for non-RAD techniques. Dose distributions were calculated using the Acuros XB algorithm with a grid size of $2.5\ mm \times\ 2.5\ mm \times\ 3\ mm$. While the 3 mm Z-axis resolution may introduce slight dosimetric uncertainty in small structures like the LAD, this grid was uniformly applied across all plans to ensure relative dosimetric comparisons remained valid.

Depending on target geometry, eight to nine fields with sliding window and coplanar arrangements were applied in IMRT plans. To address the complexity of treating the chest wall including internal mammary nodes while strictly sparing the lungs and heart, a highly modulated VMAT approach was employed. The

VMAT plans utilized five partial arcs rotating from 300° to 350°, 350° to 300°, 330° to 170°, 160° to 0°, and 20° to 160°, respectively (Fig. 4 **(B)**). This multi-arc arrangement was chosen to maximize the degrees of freedom for the optimizer to carve dose away from the coronary substructures. Collimator angles were fixed at 15° or 345° to enhance modulation capabilities and minimize interleaf leakage.

In the Eclipse, RAD treatment planning utilized user-defined static angle modulated ports (STAMPs) positioned at specific angles. This hybrid methodology is designed to potentially decrease the time required for both algorithmic optimization and actual treatment delivery. Through STAMPs, users can modulate the ratio of arc-based to static field components. This balance is managed via a five-point weighting scale: “arc dominant” (-2), “arc” (-1), “balanced” (0), “static” (+ 1), and “static dominant” (+ 2). In this study, all RAD plans were optimized using a weighting of “balanced” (0) to evenly share the proportion of weights between static ports and arc therapy during plan optimization. Furthermore, with 6 gantry pauses strategically set at 120°, 140°, 160°, 300°, 315°, and 330°, all RAD plans were generated using two arcs spanning 300° to 170°, delivered in clockwise and counter-clockwise directions, respectively. To maximize MLC modulation capability, collimator rotation for all plans was automatically optimized within Eclipse.

Plan evaluation

To ensure a consistent comparison, all plans were normalized so that 95% of the PTV received 50 Gy. Each technique was then evaluated and compared using standardized dose metrics and DVHs from the planning protocol. Furthermore, dose metrics of relevant cardiac substructures that may lead to radiation-induced effects and suggested by literatures [1, 5, 8, 19–25] were also evaluated and are listed in Table 2. The LCX was excluded from the evaluation due to the inherent difficulty of achieving accurate delineation using CT images alone. This decision aligns with previous findings in the literature [16, 26, 27], which note that the LCX often appears discontinuous across axial slices - an artifact likely attributed to the variable position of the atrioventricular (AV) groove during scanning.

Table 2
Dose metrics of cardiac substructures (with corresponding radiation-induced effects) evaluated in this research.

Substructure	Dose metrics	Effects
LV	D_{mean}	Global longitudinal strain (GLS) decreasing [5]
	V_5	Increasing of acute coronary events [19]
	V_{25}	Increasing of major ischemic events [8]
LAD	D_{mean}	Risk of Radiation-induced atherosclerosis rising [20]
	D_{max}	Risk of acute necrosis of the vessel wall and thrombosis rising [8, 20]
	V_{15}	Increasing of all-cause mortality and major adverse coronary events [21, 22]
	V_{30}	Increase major cardiac events [23, 24]
LA	V_5, V_{20}, V_{45}	Independent overall survival (OS) predictors [1]
To assess the spatial agreement of dose distributions across the three radiotherapy techniques, the conformity index (CI) was computed for every plan. Based on established definitions [28–30], the index is calculated as:		

$$CI = \frac{TV_{PTV}^2}{TV \times PIV} \#(1)$$

Where the TV_{PTV} denotes the portion of the target volume encompassed by the prescription isodose line. TV and PIV correspond to the prescription isodose volume and the total target volume, respectively. A CI value approaching 1 signifies ideal dose conformity.

Additionally, plan complexity was quantified using the modulation complexity score (MCS). Adhering to the protocol by Masi et al. [31], the MCS integrates aperture area variability (AAV) and leaf sequence variability (LSV) across all control points, weighted by monitor units (MUs). To provide a comprehensive metric involving leaf dynamics, a multiplicative index of leaf travel (LT) and MCS, termed LTMCS, was also derived:

$$LTi = \frac{1000 - LT}{1000} \quad and \quad LTMSC = LTi \bullet MCS \#(3)$$

The higher complexity of a plan, a lower MSC and LTMSC would be calculated.

Normal tissue complication probabilities (NTCP) were calculated using the Lyman-Kutcher-Burman (LKB) model for endpoint events and corresponding parameters listed in Table 3. The LKB model can be expressed as [32]:

$$NTCP = \frac{1}{\sqrt{2\pi}} \int_{-\infty}^{t} e^{-\frac{x^2}{2}} dx \ \#(4)$$

And:

$$t = \frac{EUD - TD_{50}}{m \bullet TD_{50}} \quad and \quad EUD = \left(\sum {}_i v_i D_i^{\frac{1}{n}} \right)^n \#(5)$$

Where the D_{50} represent the uniform dose causing a 50% complication probability, m stands for the slope of the curve, and n describes the importance of the volume effect. Table 3 listed all used parameters in NTCP calculation. It must be explicitly caveated that several LKB parameters utilized are based on lung, oesophageal, or mediastinal tumour populations; thus, their absolute applicability to breast cancer requires cautious interpretation.

All statistical tests in this research were performed by Wilcoxon Signed-Rank test [33] with significance level of 0.05, and multiple comparisons are corrected by Benjamini-Hochberg (BH) procedure [34].

Table 3
Parameters used in NTCP calculation.

Endpoint event	**TD_{50}**	**m**	**n**
Long term cardiac (LT-CVD) mortality [16]	52.3	0.28	1
Pericarditis/pericardial effusion (Peff) [35]	50.6	0.13	0.64
Cardiac perfusion defects (PD) [36]	12	0.6	1
Symptomatic pericardial effusion (sPCE) [37]	57.7	0.19	0.36
LV PD [38]	29	0.41	0.16
LA major adverse cardiac events (MACE) [39]	43.3	0.59	0.78
LAD toxicity [40, 41]	48	0.1	0.35
Pulmonary pneumonitis [42]	30.8	0.37	0.99

Results

Total 60 of RAD, IMRT, and VMAT plans were generated. After normalization (ensuring 95% of the PTV received 50 Gy), the $D_{99\%}$ of all plans reached prescribed dose, and all plans satisfied all hard dose constraints (**Table-1**), except 5 IMRT plans which violated D_{mean} < 8 Gy constraint for the heart. For the five excluded IMRT plans, anatomical evaluations revealed that the average overlapping area between the PTV and the heart was larger than that of the remaining cohort (mean $\pm$ SD: 1.48 CC $\pm$ 1.10 CC for excluded plans vs. 0.46 CC $\pm$ 0.86 CC for remaining plans). Furthermore, the PTV shapes in these five excluded cases were observed to be more curved and in closer physical proximity to the heart. These anatomically challenging baseline characteristics could potentially explain why these specific

IMRT plans resulted in higher mean heart doses and failed to meet the required constraints. To ensure fairness, these five plans were excluded from the following plan analysis and comparison. **S-Table 1** illustrates the average dosimetric metrics for all 20 IMRT plans. The exclusion of the five non-compliant IMRT plans artificially lowered the majority of the average dosimetric metrics for the IMRT cohort, except for the spinal cord D_{max}, right lung V_5, and right breast V_3, V_5, and D_{mean}. For all 55 qualified plans, **S-Table 2** and **S-Table 3** listed the average dosimetric metrics and P values from pairwise statistical comparisons (adjusted using the Benjamini-Hochberg (BH) procedure), respectively. Regarding planning aims, the MHD of 2 RAD, 18 IMRT, and 17 VMAT plans exceed 4 Gy, while the mean right breast dose of 9 RAD, 0 IMRT, and all VMAT plans exceed 4 Gy.

Figure-1 summarizes the comparative dosimetric analysis. RAD plans demonstrated significantly lower ($P < 0.05$) dose metrics for the spinal cord, left lung, and heart compared to both IMRT and VMAT plans. For the right lung and right breast, RAD doses were significantly lower ($P < 0.05$) than VMAT, though IMRT achieved the lowest doses among the three modalities. In terms of cardiac substructures, RAD plans demonstrated significantly lower ($P < 0.05$) values for most evaluated dose metrics compared to IMRT and VMAT plans. The V_5, V_{20} and V_{45} of LA for all plans were approximately equal to 0, indicating superior LA protection afforded by modern radiotherapy. Compared to IMRT plans, RAD achieved better sparing of the LAD, reducing the mean dose (mean $\pm$ SD: 28.02 Gy $\pm$ 9.96 Gy for RAD vs. 37.31 Gy $\pm$ 10.66 Gy for IMRT), V_{30} (55% $\pm$ 26% for RAD vs. 77% $\pm$ 27% for IMRT), and V_{40} (25% $\pm$ 23% for RAD vs. 68% $\pm$ 28% for IMRT). Furthermore, as demonstrated in **S-Table 1** and Fig. 1, comparing RAD against the complete 20-patient IMRT cohort reveals an even wider dosimetric advantage in favor of RAD than this primary 15-patient comparison.

Figure 2 presents the mean DVH with 95% confidence intervals for OARs and cardiac substructures. RAD plans achieved superior sparing of the left lung, upper lobe of the left lung, heart, LA, and LV compared to IMRT and VMAT. While RAD provided improved protection of the right lung and right breast relative to VMAT, it resulted in higher integral doses than IMRT. Doses to the LAD were comparable between RAD and VMAT, with both being lower than IMRT.

For the PTV, the average CI was significantly higher for RAD (0.823, $P = 0.031$) and VMAT (0.823, $P = 0.028$) compared to IMRT (0.805). Plan complexity analysis revealed that the average MCS and LTMCS for RAD (0.137 and 0.135) and IMRT (0.141 and 0.139) were significantly lower ($P < 0.001$) than for VMAT (0.251 and 0.245), indicating higher complexity in VMAT plans. Moreover, RAD plans required significantly more ($P < 0.001$) MUs than VMAT but significantly fewer ($P < 0.001$) than IMRT. It must be emphasized that MU count is merely a theoretical estimate of delivery efficiency. Because RAD necessitates strategic gantry pauses to deliver static ports, the actual overall treatment time cannot be directly inferred from MUs alone.

Figure 3 displays the average NTCP values and statistical comparisons. NTCPs for LT-CVD mortality, Peff, and sPCE were negligible. RAD plans yielded significantly lower estimated NTCPs for cardiac PD ($P < 0.01$), LA MACE ($P < 0.01$), and pulmonary pneumonitis ($P < 0.01$) compared to competing modalities.

Regarding LA MACE, it should be noted that although the V_5, V_{20}, and V_{45} of the left atrium (LA) were approximately 0% across all plans, non-zero absolute mean doses (Fig. 1) translated into small but consistently shifting NTCP values when applied to the LKB model. Furthermore, compared to IMRT, RAD demonstrated significantly lower NTCPs for LV PD ($P < 0.001$) and LAD toxicity ($P < 0.001$). While VMAT showed significantly lower ($P < 0.001$) NTCPs for Cardiac PD, LV PD, LA MACE, and LAD toxicity compared to IMRT, its NTCP for pulmonary pneumonitis was comparable to IMRT.

Figure 4 illustrates the comparative dose distributions for a representative patient. Visual inspection confirms that RAD substantially constrains the low-dose bath within the lung and heart relative to VMAT and IMRT. Conversely, both RAD and VMAT resulted in increased low-dose spillage to the contralateral breast compared to IMRT.

Discussion

This study contributes the first comprehensive assessment of the RAD technique applied to left-sided chest radiotherapy, benchmarked against standard IMRT and VMAT modalities. As illustrated in Figs. 1, 2, and 4, RAD achieves superior dose sparing for ipsilateral OARs (heart and left lung) while maintaining robust target coverage, which imply that RAD facilitates the intensified modulation in critical sectors required for OAR sparing.

Notably, although IMRT is traditionally favoured for minimizing low-dose spillage (V_5) compared to rotational modalities [43, 44], our results indicate that RAD yielded a comparable left lung V_5 and a significantly reduced ($P < 0.05$) V_{20} compared to IMRT (Fig. 1). Moreover, the V_{20} of the left lung - a robust predictor of symptomatic radiation pneumonitis (RP) and long-term pulmonary fibrosis - was significantly lower ($P < 0.001$) in RAD plans compared to other modalities (Fig. 1). This finding is particularly notable given that the literature typically cites V_{20} reduction as the physical advantage of VMAT [45, 46]. Furthermore, segmental analysis revealed that RAD provides enhanced protection for the left upper lung lobe compared to both VMAT and IMRT.

As illustrated in Fig. 4, IMRT and VMAT inevitably resulted in collateral cardiac exposure due to the anatomical alignment required to ensure adequate coverage of the internal mammary lymph nodes. Conversely, RAD mitigated this geometric challenge, yielding a significant reduction ($P < 0.05$) in MHD and superior sparing of cardiac substructures, as showed in Figs. 1, 2 **((F), (G), and (H))**, and **3**. When interpreted through the dose-response mechanisms detailed in Table 2, this statistical dosimetric superiority suggests potential benefits; however, these findings remain purely theoretical and require rigorous clinical validation before any actual reduction in toxicity can be assumed. These improved outcomes are likely attributable to the capacity of RAD to arrest gantry rotation, facilitating intensified leaf modulation specifically when the beam aligns with the cardiac interface.

To further quantify the clinical impact of these dosimetric gains, NTCP modelling was performed using the LKB model. Significantly lower ($P < 0.05$) NTCP values for cardiac perfusion defects, LA MACE, and

pulmonary pneumonitis were reported in RAD plans compared to IMRT and VMAT plans (Fig. 3). It is also noteworthy that while VMAT achieved lower cardiac toxicity probabilities than IMRT, it did not offer a similar benefit for pulmonary pneumonitis, whereas RAD consistently minimized predicted complications for both cardiac and pulmonary systems. Mechanistically, this is likely associated with the static ports decreasing low-dose lung exposure compared to continuous arcs.

Consistent with results reported in the literature [47–49], VMAT exhibited significantly improved ($P < 0.05$) dose conformity (average CI: 0.823 vs. 0.805), heart and left-sided lung protection, and reduced MUs compared to IMRT plans (Figs. 1 and 2). However, due to the “low-dose bath” effect, VMAT plans delivered higher doses to contralateral OARs, which may be associated with a potential secondary cancer risk—a concern for young patients. Nevertheless, RAD resulted in significantly lower ($P < 0.05$) contralateral doses compared to VMAT, implying that the static ports utilized in RAD assist in mitigating the “low-dose bath” typically associated with full arc therapies, offering an intermediate solution superior to VMAT.

RAD demonstrated a high CI, comparable to VMAT and superior to IMRT, ensuring that the high-dose region remains tightly restricted to the PTV. In terms of delivery efficiency, RAD plans required fewer MUs than IMRT, though the count exceeded that of VMAT. The complexity analysis - indicated by lower MCS and LTMCS - suggests that RAD plans possess a higher degree of complexity than VMAT. This elevated complexity represents a necessary compromise to achieve the enhanced modulation required to divert dose from cardiac structures. However, given the significant reduction ($P < 0.05$) in NTCPs, the moderate increase in MUs and complexity relative to VMAT could be considered as clinically justified.

Notably, five IMRT plans failed to satisfy the strict mean heart dose (MHD) constraint (< 8 Gy), whereas the corresponding RAD and VMAT plans for these same patients successfully met all dosimetric criteria. This discrepancy indicates that in cases involving unfavourable anatomy—specifically where the target volume is in close proximity to the heart—IMRT may reach its modulation limits more rapidly than arc-based therapies. Crucially, the exclusion of these non-compliant plans underestimates the true dosimetric disadvantage of IMRT, making the observed superiority of RAD in cardiac sparing even more pronounced.

This study has several limitations. First, the cohort size ($n = 20$) is relatively small, which inherently limits the robustness and broad generalizability of the findings. Consequently, the reported dosimetric superiority of RAD should be interpreted with caution until validated across larger, multi-centre cohorts. Second, NTCP modelling relies on LKB parameters derived from heterogeneous patient cohorts (lung cancer, lymphoma, and breast cancer). While we utilized the most relevant available parameters for breast cancer patients (Table 3), these estimates should be interpreted as relative metrics for plan ranking rather than absolute predictors of clinical toxicity. Future studies with larger cohorts and long-term follow-up are necessary to validate these radiobiological predictions. Third, results of this study from a single institution using Eclipse on a TrueBeam may not be generalizable to other TPS or linac platforms.

Although this study demonstrates the dosimetric advantages of RAD under free-breathing conditions, it is important to contextualize these findings alongside DIBH, which has become a standard cardiac sparing strategy in many institutions. While DIBH effectively increases the physical distance between the heart and the target volume, not all patients can tolerate or reliably reproduce breath-holds. For such patients, RAD offers a highly effective, compliance-independent alternative to mitigate cardiac exposure. Furthermore, future research should explore the potential synergistic effects of combining RAD with DIBH to achieve unprecedented cardiac substructure sparing.

Finally, as a pre-clinical dosimetric evaluation study, the physical delivery and patient-specific quality assurance (QA) of the RAD plans were not performed. The clinical implementation of RAD will necessitate rigorous, specialized QA protocols, particularly to verify the mechanical accuracy of the gantry pauses and the dosimetric stability during these static-field deliveries. Furthermore, the introduction of gantry pauses inherently prolongs the treatment duration compared to continuous VMAT. While the estimated delivery times for RAD are potentially shorter than those for traditional IMRT, the increased duration relative to VMAT introduces an elevated risk of intrafraction motion. The future research should include evaluating the true impact of this technique on daily clinical efficiency to justify its routine adoption.

Conclusions

RAD demonstrates potential as a feasible and dosimetrically superior technique for left-sided chest radiotherapy. It confers a distinct dosimetric advantage over conventional VMAT and IMRT by reducing the dose delivered to critical cardiac substructures and the left lung, leading to lower predicted NTCPs. While IMRT remains superior for contralateral tissue sparing, RAD provides an optimal balance of target conformity and ipsilateral organ protection, positioning it as a promising modality for minimizing lung and cardiac toxicity in breast cancer survivors. However, given the exploratory nature of this retrospective dosimetric study, these findings require prospective validation using clinical outcomes.

Abbreviations

AAV
Aperture Area Variability
CI
Conformity Index
CTV
Clinical Target Volume
DVH
Dose-Volume Histograms
EBRT
External Beam Radiotherapy
GTV

Gross Tumour Volume
IMRT
Intensity-modulated Radiation Therapy
LKB
Lyman-Kutcher-Burman
LAD
Left anterior Descending Coronary Artery
LV
Left Ventricle
LT-CVD
Long Term Cardiac Mortality
LCX
Left Circumflex Artery
MACE
Major Adverse Cardiac Events
MHD
Mean Heart Dose
MU
Monitor Units
MCS
Modulation Complexity Score
NTCP
Normal Tissue Complication Probability
OAR
Organ-at-Risk
PTV
Planning Target Volume
Peff
Pericardial Effusion
PD
Cardiac Perfusion Defects
RAD
RapidArc Dynamic
RA
Right Atrium
RCA
Right Coronary Artery
RV
Right Ventricle
sPCE

Symptomatic Pericardial Effusion
STAMPs
Strategically Placed Key User-selected Static Angle Modulated Ports
VMAT
Volumetric Modulated Arc Therapy
LSV
Leaf Sequence Variability
LTMSC
Leaf Travel (LT) and MCSv

Declarations

Ethics approval and consent to participate:

The requirement for ethical approval and informed consent was waived by the Ethics Committee of Shandong Cancer Hospital (Shandong Cancer Hospital and Institute, Shandong First Medical University and Shandong Academy of Medical Science) due to the retrospective nature of the study and the use of anonymized patient data. The authors confirm that all methods were performed in accordance with the relevant guidelines and regulations. This study was conducted in strict compliance with the Declaration of Helsinki.

Consent for publication:

Not Applicable

Competing Interests:

Not Applicable

Funding statement:

This study was supported by the Natural Science Foundation of Shandong (Grant ID: ZR2025QC1661), the National Natural Science Foundation of China (Grant ID: 12275162 and 12575365), and the Key Research and Development Program of Xinjiang Uygur Autonomous Region of China (Grant ID: 2022B03019-5).

Author Contribution

Yutong Zhao: Methodology; Formal analysis; Investigation; Validation; Visualization; Data Curation; Project administration; Writing – Original Draft; Writing - Review & EditingXinqiang Zhang: Methodology; Resources; Data Curation; Writing - Review & Editing; Project administrationXiaoshen Wang: Methodology; Formal analysis; Resources; Writing - Review & EditingZejun Jiang: Resources; Data CurationJinzhi Wang: Conceptualization; MethodologyHonan Xiao: Conceptualization; MethodologyGuanzhong Gong: Conceptualization; Writing - Review & Editing; SupervisionYong Yin; Conceptualization; Writing - Review & Editing; Supervision

Acknowledgement

The authors wish to express their sincere gratitude to Dr. Pejman Rowshanfarzad (The University of Western Australia) and Prof. Martin A. Ebert (Sir Charles Gairdner Hospital, The University of Western Australia) for their invaluable guidance and expertise, which were instrumental in the execution of this research and the preparation of the manuscript. Their insightful feedback greatly enhanced the quality of this work.

Data Availability

Available with restricted access:The data that support the findings of this study are available from Shandong Cancer Hospital and Institute (Shandong First Medical University and Shandong Academy of Medical Science), but restrictions apply to the availability of these data, which were used under licence for the current study and so are not publicly available. The data are, however, available upon request and with the permission of Shandong Cancer Hospital and Institute (Shandong First Medical University and Shandong Academy of Medical Science).

References

1. Li X, et al. Radiation-induced cardiac substructure damage and dose constraints: a review. Radiat Oncol. 2025;20(1):94.
2. Banfill K, et al. Cardiac toxicity of thoracic radiotherapy: existing evidence and future directions. J Thorac Oncol. 2021;16(2):216–27.
3. Luo Y et al. *Reflecting on the cardiac toxicity in non-small cell lung cancer in the era of immune checkpoint inhibitors therapy combined with thoracic radiotherapy.* Biochimica et Biophysica Acta (BBA)-Reviews on Cancer, 2023. 1878(6): p. 189008.
4. Darby SC, et al. Risk of ischemic heart disease in women after radiotherapy for breast cancer. N Engl J Med. 2013;368(11):987–98.
5. Piroth MD, et al. Heart toxicity from breast cancer radiotherapy: Current findings, assessment, and prevention. Strahlenther Onkol. 2019;195(1):1–12.

6. Prunaretty J, et al. Different meaning of the mean heart dose between 3D-CRT and IMRT for breast cancer radiotherapy. Front Oncol. 2023;12:1066915.
7. Jacob S, Kirova Y, Marijon E. Beyond Mean Heart Dose: Rethinking Cardiac Dysfunction and Risk Assessment in Breast Radiation Therapy. Washington DC: American College of Cardiology Foundation; 2025. pp. 231–3.
8. Bowen Jones S, et al. Moving beyond mean heart dose: The importance of cardiac substructures in radiation therapy toxicity. J Med Imaging Radiat Oncol. 2024;68(8):974–86.
9. Berlin E, et al. Cardiac effects of modern breast radiation therapy in patients receiving systemic cancer therapy. Cardio Oncol. 2025;7(3):219–30.
10. Perman M, et al. Doses to the right coronary artery and the left anterior descending coronary artery and death from ischemic heart disease after breast cancer radiotherapy: a case-control study in a population-based cohort. Acta Oncol. 2024;63:19677.
11. Lai T-Y, et al. Association of radiation dose to cardiac substructures with major ischaemic events following breast cancer radiotherapy. Eur Heart J. 2023;44(45):4796–807.
12. Clark R et al. Comparison of advanced dynamic Arc therapy with collimator rotation and fixed integrated gantry positions to the standard of care across five treatment sites. Cureus, 2025. 17(6).
13. Taylor C, et al. Estimating the risks of breast cancer radiotherapy: evidence from modern radiation doses to the lungs and heart and from previous randomized trials. J Clin Oncol. 2017;35(15):1641–9.
14. Group EBCTC. Effects of radiotherapy and of differences in the extent of surgery for early breast cancer on local recurrence and 15-year survival: an overview of the randomised trials. Lancet. 2005;366(9503):2087–106.
15. Yucheng L, et al. Development and validation of a deep reinforcement learning algorithm for auto-delineation of organs at risk in cervical cancer radiotherapy. Sci Rep. 2025;15(1):6800.
16. Feng M, et al. Development and validation of a heart atlas to study cardiac exposure to radiation following treatment for breast cancer. Int J Radiation Oncology* Biology* Phys. 2011;79(1):10–8.
17. eviQ. Breast invasive cancer adjuvant EBRT post-mastectomy. 2024 28 March 2024 [cited 2025 29 December]; Available from: https://www.eviq.org.au/radiation-oncology/breast/1925-breast-invasive-cancer-adjuvant-ebrt-post-mas
18. Gradishar WJ, et al. Breast cancer, version 3.2022, NCCN clinical practice guidelines in oncology. J Natl Compr Canc Netw. 2022;20(6):691–722.
19. van den Bogaard VA, et al. Validation and modification of a prediction model for acute cardiac events in patients with breast cancer treated with radiotherapy based on three-dimensional dose distributions to cardiac substructures. J Clin Oncol. 2017;35(11):1171–8.
20. Honaryar MK, et al. Early Development of atherosclerotic plaques in the coronary arteries after Radiotherapy for breast Cancer (BACCARAT study). J Cardiovasc Dev Disease. 2023;10(7):299.

21. Atkins KM, et al. Association of left anterior descending coronary artery radiation dose with major adverse cardiac events and mortality in patients with non–small cell lung cancer. JAMA Oncol. 2021;7(2):206–19.
22. Bradley JD, et al. Standard-dose versus high-dose conformal radiotherapy with concurrent and consolidation carboplatin plus paclitaxel with or without cetuximab for patients with stage IIIA or IIIB non-small-cell lung cancer (RTOG 0617): a randomised, two-by-two factorial phase 3 study. Lancet Oncol. 2015;16(2):187–99.
23. Skyttä T, et al. Troponin T-release associates with cardiac radiation doses during adjuvant left-sided breast cancer radiotherapy. Radiat Oncol. 2015;10(1):141.
24. Wang X, et al. The impact of radiation dose to heart substructures on major coronary events and patient survival after chemoradiation therapy for esophageal cancer. Cancers. 2022;14(5):1304.
25. Honaryar M, et al. Cancer therapy-related cardiac dysfunction after radiation therapy for breast cancer: results from the BACCARAT cohort study. Cardio-Oncology. 2024;10(1):54.
26. Milo MLH, et al. Delineation of whole heart and substructures in thoracic radiation therapy: National guidelines and contouring atlas by the Danish Multidisciplinary Cancer Groups. Radiother Oncol. 2020;150:121–7.
27. Duane F, et al. A cardiac contouring atlas for radiotherapy. Radiother Oncol. 2017;122(3):416–22.
28. Gonultas L, Dirican B. The novel universal conformity index and unconformity index algorithms for radiotherapy treatment plans. Med Dosim. 2022;47(3):295–300.
29. Menon SV, et al. Evaluation of plan quality metrics in stereotactic radiosurgery/radiotherapy in the treatment plans of arteriovenous malformations. J Med Phys. 2018;43(4):214–20.
30. Paddick I. A simple scoring ratio to index the conformity of radiosurgical treatment plans. J Neurosurg. 2000;93(supplement3):219–22.
31. Masi L, et al. Impact of plan parameters on the dosimetric accuracy of volumetric modulated arc therapy. Med Phys. 2013;40(7):071718.
32. Kargar N, Zeinali A, Molazadeh M. Impact of dose calculation algorithms and radiobiological parameters on prediction of cardiopulmonary complications in left breast radiation therapy. J Biomedical Phys Eng. 2024;14(2):129.
33. Wilcoxon F. Individual comparisons by ranking methods. Biometrics Bull. 1945;1(6):80–3.
34. Benjamini Y, Hochberg Y. Controlling the false discovery rate: a practical and powerful approach to multiple testing. J Roy Stat Soc: Ser B (Methodol). 1995;57(1):289–300.
35. Martel MK, et al. Fraction size and dose parameters related to the incidence of pericardial effusions. Int J Radiation Oncology* Biology* Phys. 1998;40(1):155–61.
36. Das SK, et al. Predicting radiotherapy-induced cardiac perfusion defects. Med Phys. 2005;32(1):19–27.
37. Fukada J, et al. Mean heart dose-based normal tissue complication probability model for pericardial effusion: a study in oesophageal cancer patients. Sci Rep. 2021;11(1):18166.

38. Ma J, et al. Post mastectomy linac IMRT irradiation of chest wall and regional nodes: dosimetry data and acute toxicities. Radiat Oncol. 2013;8(1):81.
39. Lai T-Y, et al. Estimating the risk of major adverse cardiac events following radiotherapy for left breast cancer using a modified generalized Lyman normal-tissue complication probability model. Breast. 2024;77:103788.
40. Mężeński P, Kukołowicz P. What new dose distribution statistics may be included in the optimization of dose distribution in radiotherapy for post-mastectomy patients. Nowotwory J Oncol. 2021;71(5):267–73.
41. Ma C, et al. Dosimetric comparison and evaluation of three radiotherapy techniques for use after modified radical mastectomy for locally advanced left-sided breast cancer. Sci Rep. 2015;5(1):12274.
42. Seppenwoolde Y, et al. Comparing different NTCP models that predict the incidence of radiation pneumonitis. Int J Radiation Oncology* Biology* Phys. 2003;55(3):724–35.
43. Lin J-C, et al. Comparing treatment plan in all locations of esophageal cancer: volumetric modulated arc therapy versus intensity-modulated radiotherapy. Medicine. 2015;94(17):e750.
44. Li C, et al. Dosimetric comparison of four radiotherapy techniques for stage III non–small cell lung cancer. Oncol Lett. 2023;26(2):347.
45. Zhang Q, et al. Dosimetric comparison for volumetric modulated arc therapy and intensity-modulated radiotherapy on the left-sided chest wall and internal mammary nodes irradiation in treating post-mastectomy breast cancer. Radiol Oncol. 2015;49(1):91.
46. Yeh J, Cokelek M, Tacey M. Retrospective dosimetric comparison of VMAT versus t-IMRT for patients with carbon dioxide tissue expanders undergoing left sided PMRT using the recent ESTRO-ACROP target volume delineation. Int J Radiol Radiat Ther. 2022;9(1):6–12.
47. Wolff D, et al. Volumetric modulated arc therapy (VMAT) vs. serial tomotherapy, step-and-shoot IMRT and 3D-conformal RT for treatment of prostate cancer. Radiother Oncol. 2009;93(2):226–33.
48. Majumdar SKD et al. A dosimetric study comparing 3D-CRT vs. IMRT vs. VMAT in left-sided breast cancer patients after mastectomy at a tertiary care centre in Eastern India. Cureus, 2022. 14(3).
49. Chang JS, et al. Intensity modulated radiotherapy and volumetric modulated arc therapy in the treatment of breast cancer: an updated review. J breast cancer. 2022;25(5):349.

Figures

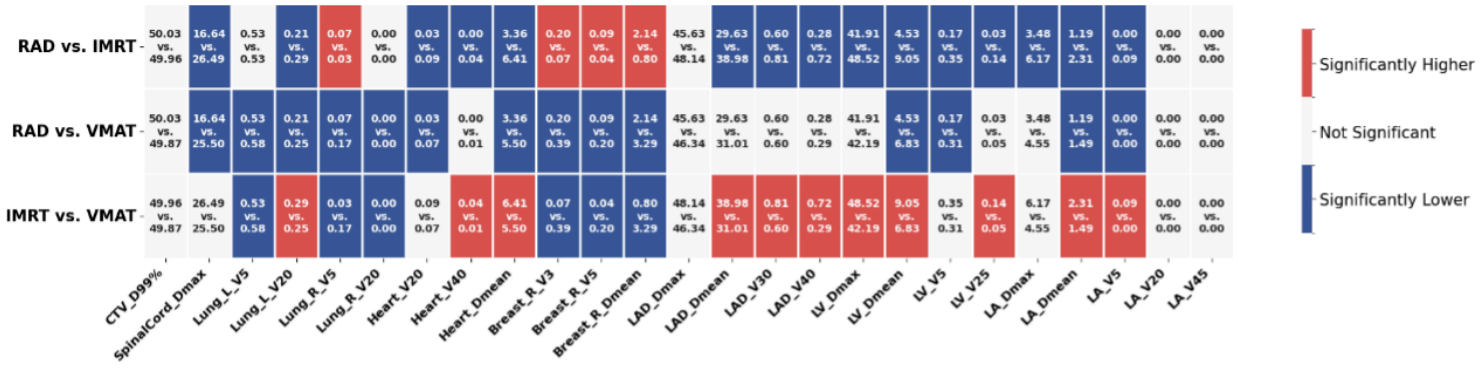


Figure 1

Statistical comparison of dosimetric metrics across radiotherapy modalities. Values within each cell represent the cohort mean. Cell coloration denotes whether the primary modality yielded a statistically higher or lower value compared to the reference modality. (Note: Comparisons involve unequal sample sizes (IMRT: n=15 vs. RAD/VMAT: n=20) due to exclusions.)

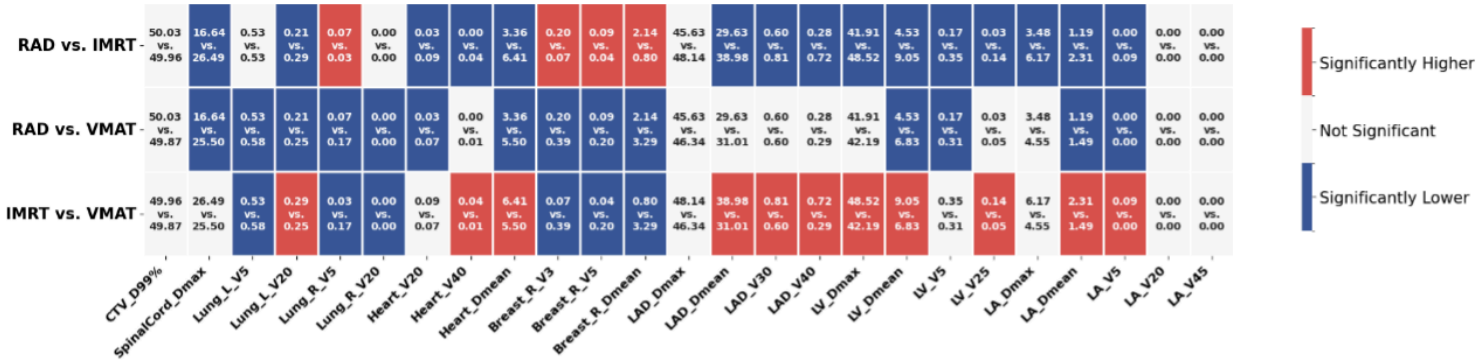


Figure 1

Statistical comparison of dosimetric metrics across radiotherapy modalities. Values within each cell represent the cohort mean. Cell coloration denotes whether the primary modality yielded a statistically higher or lower value compared to the reference modality. (Note: Comparisons involve unequal sample sizes (IMRT: n=15 vs. RAD/VMAT: n=20) due to exclusions.)

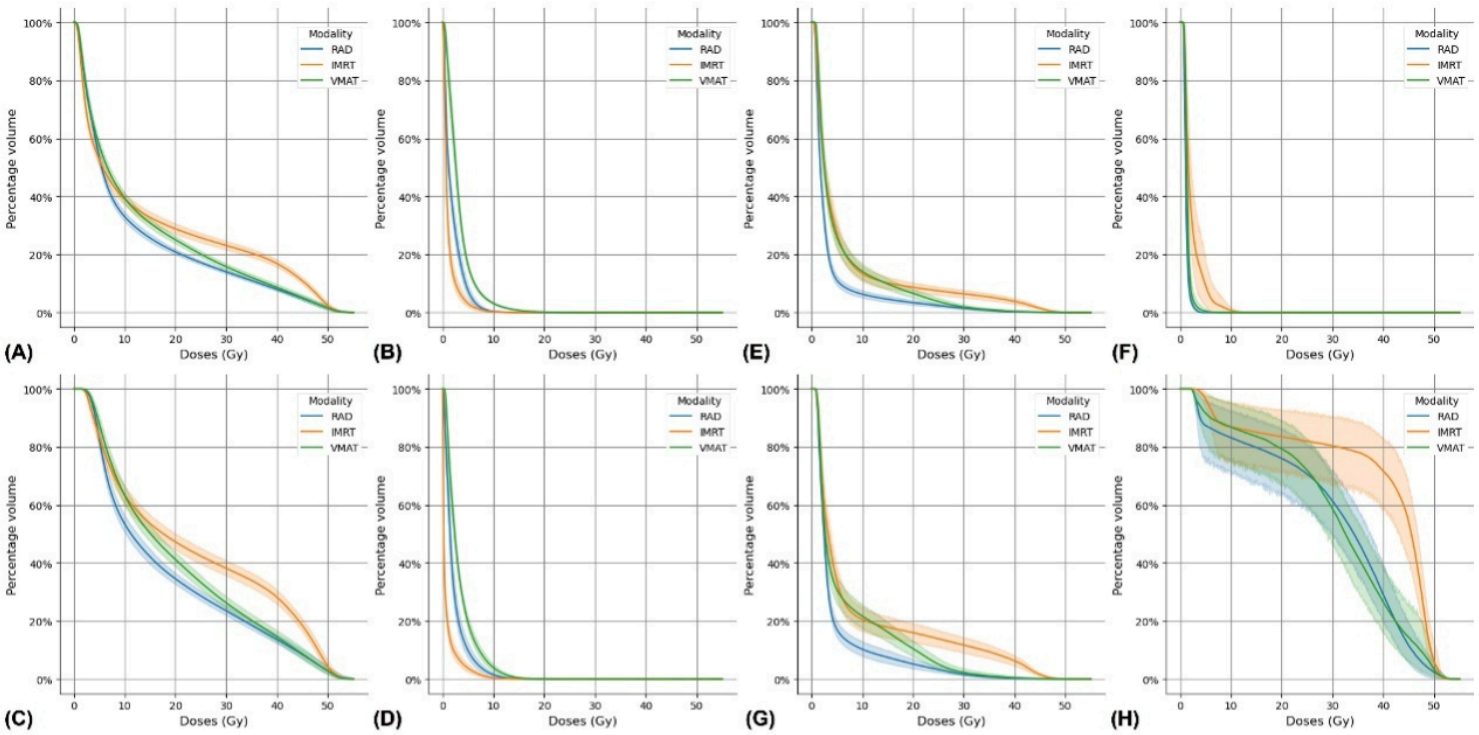


Figure 2

Mean DVH of RAD, IMRT, and VMAT plans with 95% confidence intervals for (A): left-side lung; (B): right-side lung; (C): upper lobe of left-side lung; (D): right-side of breast, (E): heart; (F): LA; (G): LV; (H): LAD. (The CIs are provided for conventional visual comparability, while all quantitative statistical claims rely on the robust non-parametric tests.)

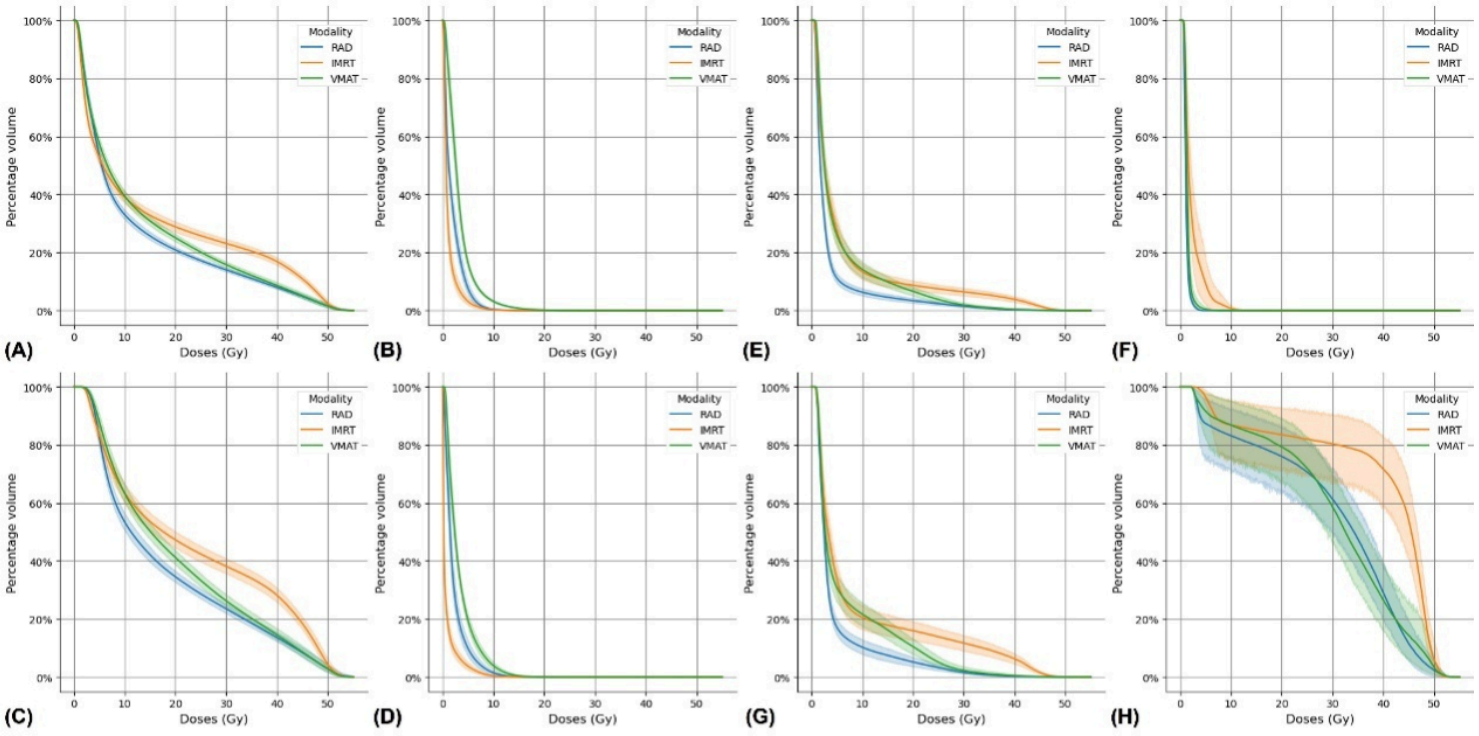


Figure 2

Mean DVH of RAD, IMRT, and VMAT plans with 95% confidence intervals for (A): left-side lung; (B): right-side lung; (C): upper lobe of left-side lung; (D): right-side of breast, (E): heart; (F): LA; (G): LV; (H): LAD. (The CIs are provided for conventional visual comparability, while all quantitative statistical claims rely on the robust non-parametric tests.)

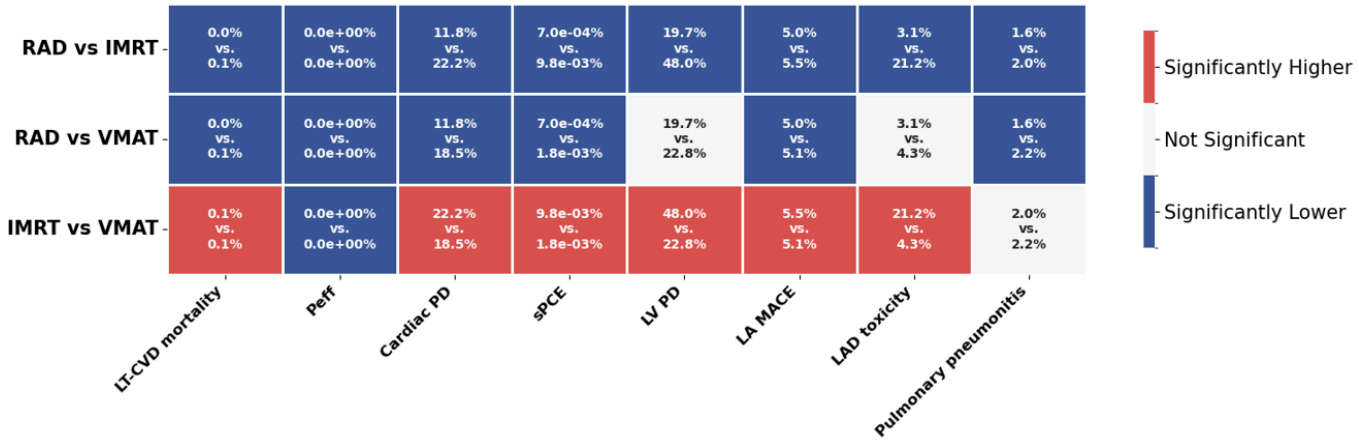


Figure 3

Average NTCP values and results of statistical comparisons for different endpoint events. Cell coloration denotes whether the primary modality yielded a statistically higher or lower value compared to the reference modality.

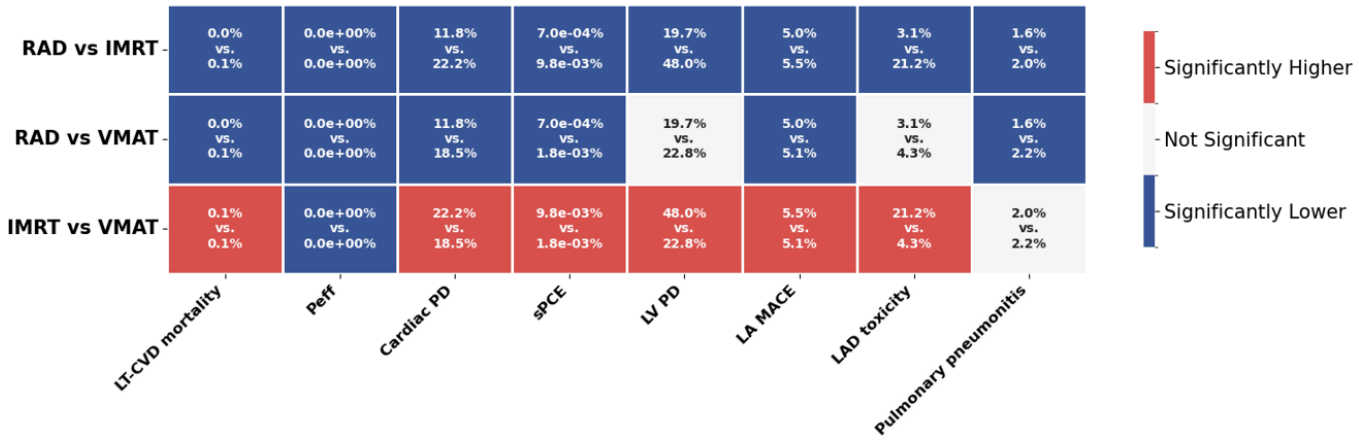


Figure 3

Average NTCP values and results of statistical comparisons for different endpoint events. Cell coloration denotes whether the primary modality yielded a statistically higher or lower value compared to the reference modality.

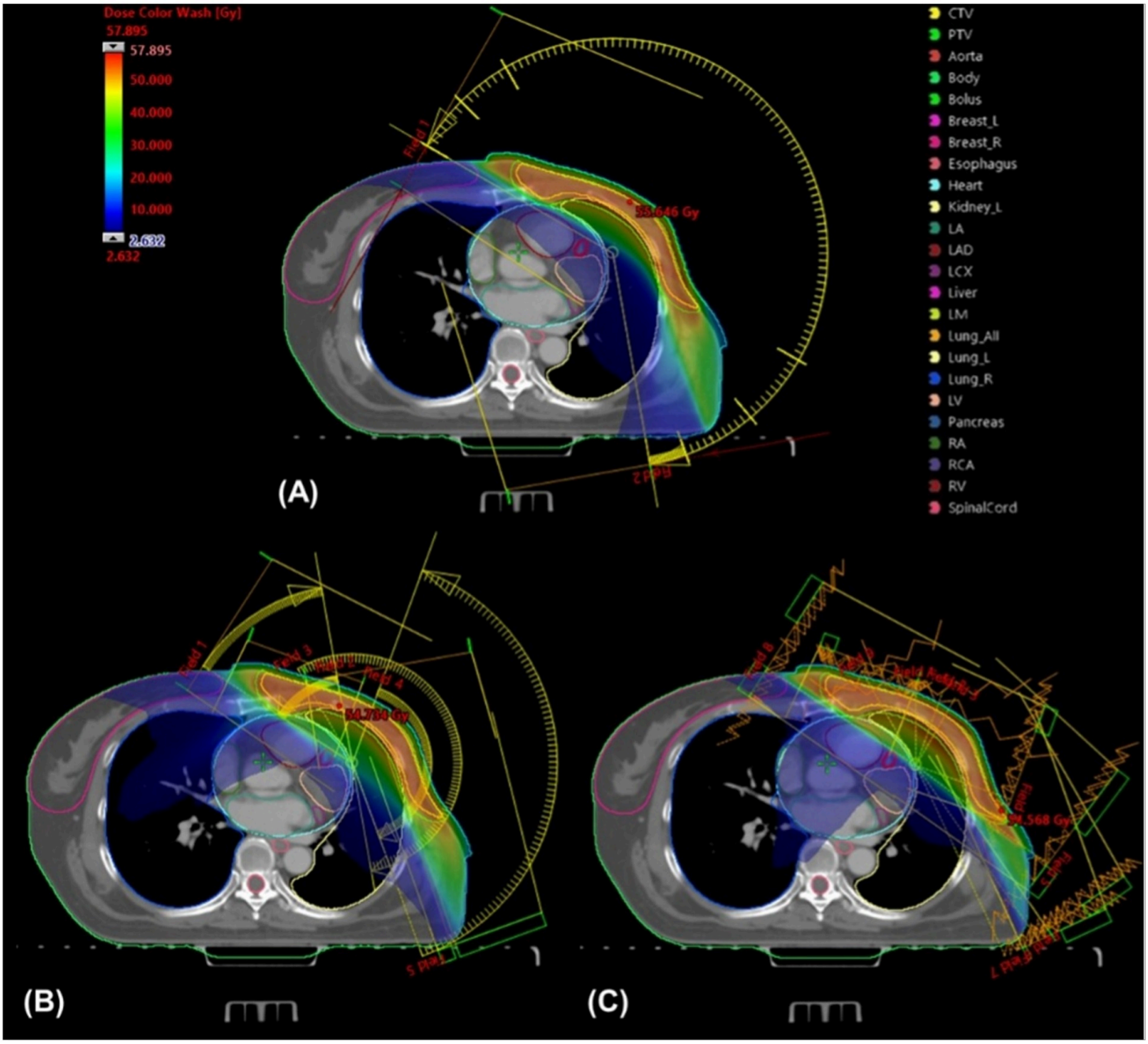


Figure 4

Dose distributions and fields arrangement of (A): RAD, (B): VMAT, and (C): IMRT plans.

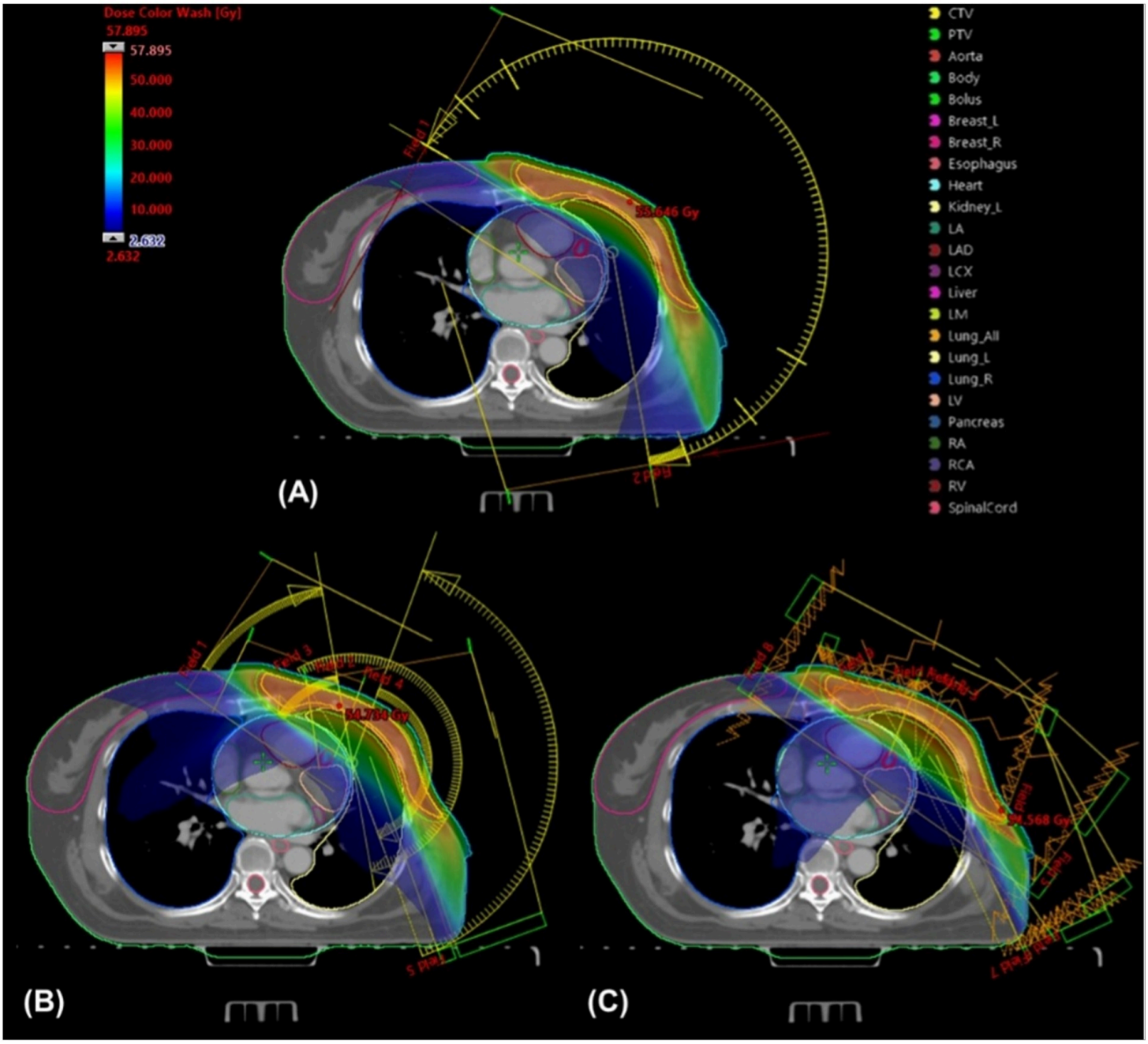


Figure 4

Dose distributions and fields arrangement of (A): RAD, (B): VMAT, and (C): IMRT plans.

Supplementary Files

This is a list of supplementary files associated with this preprint. Click to download.

- SupplementaryTables.docx
- SupplementaryTables.docx